International Journal of Engineering Science 189 (2023) 103887

Contents lists available at ScienceDirect

International Journal of Engineering Science

journal homepage: www.elsevier.com/locate/ijengsci

Bending analysis of functionally graded nanobeams based on stress-driven nonlocal model incorporating surface energy effects

Rosa Penna

Department of Civil Engineering, University of Salerno, 84084 Fisciano, Italy

ARTICLE INFO

Keywords:
Functionally graded materials
Bernoulli-Euler nanobeams
Stress-driven nonlocal model
Bending analysis
Surface energy effects

ABSTRACT

The bending response of Bernoulli-Euler nanobeams made of a functionally graded (FG) material with different cross-sectional shapes is investigated in this manuscript by a stress-driven model incorporating surface energy effects. In particular, the FG nanobeam is composed of a bulk volume and a surface layer regarded as a membrane of zero thickness perfectly adhered to the bulk continuum. The bulk material is made of a mixture of metal and ceramic, whose distributions spatially vary from the bottom to the top surface of the FG nanobeams. The nonlocal governing equations of the elastostatic bending problem are derived by using the virtual work principle. The main results of a parametric investigation are also presented and discussed varying the nonlocal parameter, the material gradient index and the boundary conditions at the ends of the nanobeams. They show how the proposed model is able to study the bending behavior of inflected FG nanobeams including surface effects.

1. Introduction

Nowadays, modeling and small-scale analysis able to describe size-dependent phenomena of ultra-small materials and structures is a topic of great interest in the emerging areas of nanotechnologies, nano-engineering and nano-sciences (Chandel et al., 2020; Dastjerdi et al., 2022; Kekic & Barisic, 2020; Rafii-Tabar et al., 2016).

Comprehensive understanding of the mechanical behavior of nanostructures including nanobeams (Malikan & Eremeyev, 2022), nanoplates and nanoshells (Shahmohammadi et al., 2023; Zheng et al., 2022) is crucial for the design and optimization of small-scale electro-mechanical devices (Akhavan et al., 2019; Cornacchia et al., 2021). Among these small-sized structures, nanobeams are basic structural elements widely used in several engineering applications like nanoactuator (Akhavan et al., 2019), nanosensors (Malikan et al., 2020), nanoresistor (Rezaiee-Pajand & Rajabzadeh-Safaei, 2022) and so on (Farajpour et al., 2022). Moreover, in order to achieve smart devices with better performance, nanobeam are often made of a functionally graded composite or nanocomposites materials (FGMs) (Ghayesh & Farajpour, 2019; Yee et al., 2023), designed and fabricated by mixing two components and their physical and mechanical properties vary gradually through preferred spatial directions to avoid typical defects related to the material discontinuities (cracking, delamination and stress concentration). Accordingly, mechanical analysis of functionally graded nanostructures (Dastjerdi et al., 2023; Eyvazian et al., 2020; Russillo et al., 2022; Xu et al., 2021) has become a very important issue that is attracting the interest of many researchers.

As has been shown in both experiments at nanoscale and atomistic simulations, size-dependency phenomena (i.e. small scale and surface phenomena) have a considerable impact in the mechanics of nanostructures. Given the intrinsic difficulties of performing

E-mail address: rpenna@unisa.it.

https://doi.org/10.1016/j.ijengsci.2023.103887
Received 8 February 2023; Received in revised form 4 May 2023; Accepted 4 May 2023
Available online 11 May 2023

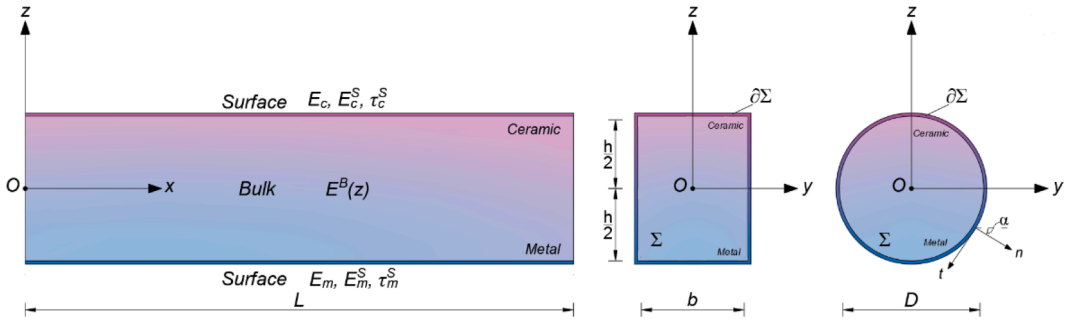

Fig. 1. Coordinate system and configuration of the FG nanobeam: bulk continuum (mixture of ceramic and metal) and surface layer for a rectangular ($b \times h$) and a circular (D) cross-section.

experiments at nanoscale level and the highly computational costs of atomistic simulations (Billinge & Levin, 2007; Lam et al., 2003; Maranganti & Sharma, 2007), two different categories of models have been proposed in the last years (Zhu & Li, 2019): the first one comprises the non-classical continuum models with the aim of describing microstructure effects, while the second one includes models incorporating surface energy phenomena. In particular, among the non-classical continuum models, the most widely applied, to name a few, are the strain gradient theory of elasticity (Mindlin, 1968), the nonlocal theory of elasticity (Eringen, 1972; Eringen, 1983), the two-phase (local/nonlocal) mixture model (Eringen, 1987) and other coupled theories of elasticity (Barretta & Marotti de Sciarra, 2019; Lim et al., 2015).

Within the framework of nonlocal theories, the Eringen's strain-driven model, originally developed to analyze surface waves and screw dislocations problems involving unbounded domain, is widely utilized in the study of the mechanical behavior of various structures at small-scale. As widely discussed in (Fernández-Sáez et al., 2016; Li et al., 2015; Romano & Barretta, 2016; Romano et al., 2017), when the strain-driven nonlocal model is applied to bounded domains, it can lead to mathematically inconsistencies due to the incompatibility between the requirements of equilibrium and the higher order constitutive boundary conditions. These problems can be bypassed using the stress-driven nonlocal model proposed by Romano and Barretta (2017) which provides a mechanically consistent approach to examine small-size structures. It is noteworthy that the stress-driven model is used to capture size effects not only in the static (Barretta et al., 2018; Barretta et al., 2018), dynamic (Apuzzo et al., 2017; Penna et al., 2021) and buckling behavior of nanobeams (Darban et al., 2020), but also to analyze nanobeams on nano-foundations (Barretta et al., 2022), FG nanobeams (Ren & Qing, 2021), nanobeams in hygro-thermal environment (Penna et al., 2021; Penna et al., 2021a, Penna et al., 2021b), curved elastic beams (Barretta et al., 2019), nanocomposite beams (Vaccaro, 2022), nanobeams in presence of loading discontinuities (Caporale et al., 2022) as well as to study the wave propagation in beam lattices (Russillo & Failla, 2022).

Moreover, unlike structures at macro-dimensional scale, for which it is possible to neglect the surface region for the study of their mechanical behavior and use the properties of the bulk as their overall properties, ultrasmall structures are characterized by a large surface area to bulk volume ratio and, therefore, the energy of the atoms near the surface is significant and leads to the formation of surface residual stresses and elastic properties other than those of the bulk (Wang et al., 2006). In order to that take into account surface energy effects, (Gurtin & Murdoch, 1975, 1978) proposed a surface elasticity theory in which the surface layer is considered as a zero-thickness membrane perfectly adhered to the bulk continuum with different material properties and constitutive laws than the bulk.

The latter theory has received great scientific interest and, increasingly, has been extensively applied to examine statical, buckling and dynamical behaviors of nanobeams (He & Lilley, 2008; Wang & Feng, 2009) where it has been observed that when the surface is modeled using positive surface elastic constants (i.e. surface young modulus, surface residual stress) the deflections decrease and the critical axial load and the natural frequency increase, while an opposite trend was seen for negative surface elastic constants.

As explained in Chen et al. (2013), surface stress is composed of two contributions: the first one is due to the intrinsic surface residual stress and the second depends on the structural deformation (or surface elasticity). It is noteworthy that the surface elastic modulus in the second contribution can be positive or negative due to the fact that a surface cannot exist without the bulk and the total energy (bulk and surface) needs to satisfy the positive definiteness condition (Shenoy, 2005).

As is well known, the non-classical continuum models and surface elasticity are employed to assess totally-different physical phenomena separately. In the current literature, the surface elasticity theory has been frequently combined with the Eringen's nonlocal elasticity (Ghadiri et al., 2016; Hashemian et al., 2019; Li et al., 2020; Li & Hu, 2022, Mahmoud, Eltaher, Alshorbagy, & Meletis, 2012) or with others higher-order continuum models (Sourani et al., 2020; Yang et al., 2023) in order to better predict the effects of surface energy and small scale on the mechanical response of homogeneous structures at nanoscale.

However, as discussed above, the Eringen's nonlocal elasticity model is inconsistent in the context of static and dynamic analyses of nanobeams and, therefore, other coupled models are needed to account for small-scale effects as well as surface phenomena.

To the author's knowledge, coupled models based on the stress-driven theory of elasticity incorporating surface energy, nonlocal parameter and material gradient index capable to capture the statical response of nanobeams made of functionally graded material are less studied. Therefore, the motivation of this paper is to propose a well-posed nonlocal approach which combines the stress-driven nonlocal model and the surface elasticity theory for the bending analysis of functionally graded straight nanobeams subjected to a

uniformly distributed load. In particular, the main results of a parametric investigation varying the nonlocal parameter, the material gradient index and the boundary conditions at the ends, are presented and discussed.

The paper is structured as follows. The problem formulation is summarized in Section 2. The stress-driven model for nanobeams and the surface elasticity theory are recalled in Section 3. Then, the nonlocal governing equations of the elastostatic bending problem are provided in Section 4. Results of the parametric analysis are discussed in Section 5. Some closing remarks are given in Section 6.

2. Problem formulation

Fig. 1 shows a functionally graded (FG) nanobeam of length L in a Cartesian coordinate system $\{O,x,y,z\}$ having the origin in the geometric center O of its cross-section Σ, being $x \quad (0 \le x \le L)$ the nanobeam axis and y, z the principal axes of geometric inertia of Σ, respectively. Moreover, let us denote by $\partial\Sigma$ the perimeter of Σ.

Two different cross-sectional shapes have been considered in the present paper: a rectangular cross-section of thickness h and width b, and a circular cross-section, with diameter D.

The FG nanobeam is composed of a bulk volume and a surface layer regarded as a zero-thickness membrane perfectly adhered to the bulk continuum. The bulk material is a metal-ceramic mixture spatially varying from the bottom surface (metal) to the top surface (ceramic). Herein and throughout this manuscript, the superscripts "B" and "S" denote the bulk continuum and surface layers of the FG nanobeam, respectively; the subscripts "c" and "m" refer to ceramic and metal, respectively.

In the current study, the Poisson's ratio is assumed to be constant ($\nu^B = \nu^S = \nu$), while bulk elastic modulus of elasticity, $E^B = E^B(z)$, surface modulus of elasticity, $E^S = E^S(z)$, and residual surface stress, $\tau^S = \tau^S(z)$, are assumed to continuously vary along transverse direction, z, according to the following power law distributions (Saffari et al., 2017)

$$E^B(z) = E_m^B + \left(E_c^B - E_m^B\right)\left(\frac{1}{2}+\frac{z}{\zeta}\right)^k \tag{1}$$

$$E^S(z) = E_m^S + \left(E_c^S - E_m^S\right)\left(\frac{1}{2}+\frac{z}{\zeta}\right)^k \tag{2}$$

$$\tau^S(z) = \tau_m^S + \left(\tau_c^S - \tau_m^S\right)\left(\frac{1}{2}+\frac{z}{\zeta}\right)^k \tag{3}$$

where $\zeta=h$ for a rectangular cross-section or $\zeta=D$ for a circular cross-section, and k denotes the gradient index of the FG material ($k \ge 0$). In particular, when $k = 0$, a homogeneous nanobeam with ceramic properties is obtained.

2.1. Displacement field

Based on the Bernoulli-Euler theory, the Cartesian components of the displacement field of the FG nanobeam along x and z directions, $u_x=u_x(x,z)$, $u_z = u_z(x,z)$, and the corresponding non-zero strain, $\varepsilon_x = \varepsilon_x(x,z)$, can be expressed, respectively, as

$$u_x(x,z) = -z\frac{\partial w(x)}{\partial x} \tag{4}$$

$$u_z(x,z) = w(x) \tag{5}$$

$$\varepsilon_x(x,z) = -z\frac{\partial^2 w(x)}{\partial x^2} \tag{6}$$

where $w = w(x)$ is the transverse displacement of the geometric center O and the term $\frac{\partial^2 w(x)}{\partial x^2}$ refers to the geometrical bending curvature χ.

3. Constitutive models

In this section, the stress–driven nonlocal model (SDM) (Romano & Barretta, 2017) is combined with the surface elasticity theory (SET) (Gurtin & Murdoch, 1975; 1978) to analyze the bending behavior of Bernoulli-Euler FG nanobeams. The proposed model is herein referred as "Surface Stress-Driven Model" (SSDM).

3.1. Stress-driven model

In adapting the general stress-driven nonlocal formulation (SDM) to the Bernoulli-Euler FG nanobeam without considering surface energy effects, the nonlocal bending curvature χ is expressed by the following convolution integral

$$\chi(x) = \int_0^L \Phi_{L_c}(x-\xi, L_c)\left(-\frac{M(\xi)}{I_E}\right) d\xi \tag{7}$$

being x and ξ the position vectors of the points of the domain, respectively.

The general expressions of the bending interaction, M, and of the second moment of elastic area, I_E, about the principal axis of geometric inertia, y, are given by the following equations

$$M = \int_\Sigma \sigma z \, d\Sigma \tag{8}$$

$$I_E = \int_\Sigma E(z)\, z^2 d\Sigma \tag{9}$$

where $E(z) = E^B(z)$ coincides, in this case, with the bulk elastic modulus of elasticity.

As is well-known, the smoothing kernel Φ_{L_c} depends on the material length-scale parameter, $L_c = \lambda_c L$, where λ_c is the dimensionless nonlocal parameter of the FG nanobeam $(\lambda_c > 0)$. By choosing a special function kernel Φ_{L_c}, required to fulfill the properties of positivity, symmetry, limit impulsivity and normalization on the real axis as (Eringen, 1983)

$$\Phi_{L_c}(x, L_c) = \frac{1}{2L_c}\exp\left(-\frac{|x|}{L_c}\right) \tag{10}$$

the convolution in Eq. (7) is equivalent to following second-order differential equation

$$\left(1 - L_c^2\frac{\partial^2}{\partial x^2}\right)\chi(x) = -\frac{M(x)}{I_E} \tag{11}$$

if and only if the following constitutive boundary conditions are satisfied at the nanobeam ends ($x = 0, L$)

$$-\frac{\partial\chi(0)}{\partial x} + \frac{1}{L_c}\chi(0) = 0 \tag{12}$$

$$\frac{\partial\chi(L)}{\partial x} + \frac{1}{L_c}\chi(L) = 0 \tag{13}$$

It can be noted that the stress-driven nonlocal formulation is well-posed and that no paradoxical results are obtained in contrast with the classical nonlocal theory (Eringen, 1972; 1983) as discussed in (Romano et al., 2017). Moreover, this model provides a consistent approach for the static, dynamic as well as post buckling analysis of nanostructures.

3.2. Surface elasticity theory

According to the surface elasticity theory, the surface of the nanobeam is modelled as a zero-thickness membrane perfectly bonded to the underlying material (bulk) and, therefore, no slipping between surface and bulk material is admitted. Moreover, bulk continuum and surface layer are characterized by different stress states: a uniaxial stress state for the bulk, given by $\sigma_x^B = \sigma_x^B(x,z)$, and a two-dimensional stress state for the surface, of components $\sigma_x^S = \sigma_x^S(x,z)$ and $\tau_{zx}^S = \tau_{zx}^S(x,z)$, respectively.

Furthermore, unlike classical Bernoulli-Euler beam theory, the component of the bulk stress in the transverse direction z, $\sigma_z^B = \sigma_z^B(x, z)$, which describes the surface layer and bulk interaction, is not negligible due to surface effects and, for a FG material, can be assumed to vary cubically along the nanobeam thickness according to the following equation (Saffari et al., 2017)

$$\sigma_z^B = f(z)\left[-\left(\tau_c^S + \tau_m^S\right)\frac{\partial^2 w}{\partial x^2}\right] + \frac{1}{2}\left[\left(\tau_c^S - \tau_m^S\right)\frac{\partial^2 w}{\partial x^2}\right] \tag{14}$$

where $f(z) = 2(z/\zeta)[(z/\zeta)^2 - 3/4]$.

Note that a linear distribution for σ_z^B is not adequate for FG nanobeams with high gradient in material properties for satisfying the surface equilibrium equations of Gurtin and Murdoch (Gurtin & Murdoch, 1975; 1978).

Now, by manipulating Eq. (14) with Eq. (6), it is obtained

$$\sigma_z^B = C\ \varepsilon_x \tag{15}$$

where the function $C = C(z)$ is given by

$$C = \frac{f(z)}{z}\left(\tau_c^S + \tau_m^S\right) - \frac{1}{2z}\left(\tau_c^S - \tau_m^S\right) \tag{16}$$

In accordance with the local formulation of the surface elasticity theory, the stress at point x is proportional to the corresponding strain at the same point. Consequently, the bulk stress-strain relation can be expressed as

$$\sigma_x^B = E^B \varepsilon_x + \nu\, \sigma_z^B = \left[E^B + \nu\, C\right] \varepsilon_x \tag{17}$$

in which the term $E^B + \nu\, C$ can be considered as an equivalent elastic modulus of elasticity taking into account surface energy effects.

For the surface layer, the two relevant constitutive relations can be formulated as

$$\sigma_x^S = \tau^S + E^S \varepsilon_x \tag{18}$$

$$\tau_{zx}^S = \begin{cases} \tau^S \dfrac{\partial u_z}{\partial x} \ (rectangular) \\ \tau^S n_z \dfrac{\partial u_z}{\partial x} \ (circular) \end{cases} \tag{19}$$

where n_z denotes the z-component of the unit normal vector $\boldsymbol{n}$, which is the outward normal to the nanobeam's lateral surface (Zhu & Li, 2019). Note that for a circular cross-section, $\boldsymbol{n} = (\cos\alpha, \sin\alpha)$ being α the angle between $\boldsymbol{n}$ and y directions (Fig. 1).

4. Elastostatic problem of inflected FG nanobeams including surface effects

In this study, the nonlocal governing equations of the elastostatic bending problem are derived by using the virtual work principle, that can be expressed as

$$\delta U + \delta W = 0 \tag{20}$$

The expression of the virtual strain (internal) energy, δU, is given by

$$\delta U = \int_0^L \left(\int_\Sigma \sigma_x^B \delta\varepsilon_x \, d\Sigma + \oint_{\partial\Sigma} \sigma_x^S \, \delta\varepsilon_x \, d\sigma \right) dx + \int_0^L \oint_{\partial\Sigma} \tau_{zx}^S \, \delta\gamma_z \, d\sigma dx = -\int_0^L M \frac{\partial^2 \delta w}{\partial x^2} dx + \int_0^L \mathrm{T}^S \frac{\partial w}{\partial x} \frac{\partial \delta w}{\partial x} dx \tag{21}$$

where $\gamma_z = \frac{\partial w}{\partial x}$ for a rectangular cross-section and $\gamma_z = n_z \frac{\partial w}{\partial x}$ for a circular cross-section, and M and T^S can be expressed as follows

$$M = \int_\Sigma \sigma_x^B \, z \, d\Sigma + \oint_{\partial\Sigma} \sigma_x^S \, z \, d\sigma \tag{22}$$

$$\mathrm{T}^S = \begin{cases} \oint_{\partial\Sigma} \tau^S d\sigma \ (rectangular) \\ \oint_{\partial\Sigma} \tau^S n_z d\sigma \ (circular) \end{cases} \tag{23}$$

It can be noted that the quantity T^S is a constant, whose expression, for FG nanobeams is given by

$$\mathrm{T}^S = \begin{cases} 2\mathrm{b}\tau_c^S + \dfrac{2\mathrm{h}\left(\mathrm{k}\tau_m^S + \tau_c^S\right)}{1+\mathrm{k}} \ (\text{rectangular}) \\ \dfrac{\pi \mathrm{D}}{2}\left(\tau_m^S - \dfrac{2\left(1+\mathrm{k}+\mathrm{k}^2\right)\sqrt{\pi}\left(\tau_m^S - \tau_c^S\right)\mathrm{Seck}\ \pi}{..(1/2-\mathrm{k}\ )..(3+\mathrm{k})} \right) \ (\text{circular}) \end{cases} \tag{24}$$

where Γ denotes the Euler gamma function. For a homogenous material ($\tau_m^S = \tau_c^S = \tau^S$), T^S becomes equal to $\mathrm{T}^S = 2(b+h)\tau^S$ for a rectangular cross-section (Sourani et al., 2020) and $\mathrm{T}^S = \pi D/2\tau^S$ for a circular cross-section (Zhu & Li, 2019).

The virtual external energy, δW, due to the applied load, $q_z = q_z(x)$, can be expressed by

$$\delta W = -\int_0^L q_z \delta w \, dx \tag{25}$$

By substituting Eq. (21) and Eq. (25) into Eq. (20) and applying the fundamental Lemma of variational calculus, the following governing equation can be obtained

$$\frac{\partial^2 M}{\partial x^2} + \mathrm{T}^S \frac{\partial^2 w}{\partial x^2} + q_z = 0 \tag{26}$$

The corresponding boundary conditions at the FG nanobeam ends ($x = 0, L$) can be chosen by specifying one element of each of the following two pairs of standard boundary conditions, SBCs (kinematic and static boundary conditions)

$$w \text{ or } \frac{\partial M}{\partial x} + \mathrm{T}^S \frac{\partial w}{\partial x} \tag{27}$$

$$-\frac{\partial w}{\partial x} \text{ or } M \tag{28}$$

Now, by substituting Eqs. (17),18 into Eq. (22) and considering Eq. (6), the following expression of the resultant moment is obtained

$$M = -I_E^* \chi + M^\tau \tag{29}$$

being $M^\tau = \oint_{\partial\Sigma} \tau^S z d\sigma$ and I_E^* the equivalent bending stiffness defined as

$$I_E^* = \int_\Sigma \left[E^B + \nu\ C\right] z^2 d\Sigma + \oint_{\partial\Sigma} E^S z^2 d\sigma \tag{30}$$

The expressions of M^τ for the two cross-sectional shapes considered in this paper are given by

$$\mathrm{M}^\tau = \begin{cases} \dfrac{h^2 k\left(\tau_m^S - \tau_c^S\right)}{(1+k)(2+k)} + bh\tau_c^S \ (rectangular) \\ \dfrac{D^2 k \pi^{3/2}\left(-\tau_m^S + \tau_c^S\right) \mathrm{Sec}\ k\pi}{2\,\Gamma(1/2-k)\Gamma(2+k)} \ (circular) \end{cases} \tag{31}$$

and the expressions of I_E^*, for the two cross-sectional shape here considered, are the following

- *rectangular cross-section*

$$I_E^* = \frac{1}{60(1+k)(2+k)(3+k)} h^2 \left(30bE_c^S(1+k)(2+k)(3+k) + 15bE_c^B h\left(2+k+k^2\right) + 5bE_m^B hk(8+k(3+k)) + 10h\left(3E_c^S\left(2+k+k^2\right) + E_m^S k(8+k(3+k))\right) - 6b(1+k)(2+k)(3+k)\nu\left(\tau_m^S + \tau_c^S\right)\right) \tag{32}$$

- *circular cross-section*

$$I_E^* = \frac{1}{256} D^3 \pi\left(4DE_m^B + 32\tau_m^S - 5\nu\left(\tau_m^S + \tau_c^S\right)\right) - \frac{1}{256} D^3 \pi \left(\frac{32\left(2\left(\tau_m^S - E_c^B\right)(3+k)(4+k)\left(1+k+k^2\right)\right)}{\Gamma(1/2-k)\Gamma(5+k)}\right) - \frac{1}{256} D^3 \pi \left(\frac{\left(D\left(E_m^B - E_c^B\right)(1+2k)\left(3+k+k^2\right)\right)\sqrt{\pi}\,Sec\ k}{\Gamma\left(\frac{1}{2}-k\right)\Gamma(5+k)}\right). \tag{33}$$

In the case of a homogenous material ($E_m^S = E_c^S = E^S; E_m^B = E_c^B = E^B; \tau_m^S = \tau_c^S = \tau^S$), Eqs. (31) reduce to Eqs. (34)

$$M^\tau = \begin{cases} bh\ \tau^S \ (rectangular) \\ 0 \ (circular) \end{cases} \tag{34}$$

while Eqs. (32) and 33 became Eqs. (35)

$$I_E^* = \begin{cases} \dfrac{bh^3}{12} E - \dfrac{bh^2}{5}\nu\ \tau^S + \left(\dfrac{h^3}{6} + \dfrac{bh^2}{2}\right) E^S \ (rectangular) \\ \dfrac{\pi D^4}{64}\mathrm{E} - \dfrac{5\pi D^3}{128}\nu\ \tau^S + \dfrac{\pi D^3}{8} E^S \ (circular) \end{cases} \tag{35}$$

Note that if the Poisson's effect is neglected, the expressions of Eq. (35) coincide with those given in (Hui & Gang-Feng, 2011).

4.1. Stress-driven model incorporating surface energy effects

In order to incorporate surface energy effects in the stress-driven model, the integral convolution law of Eq. (7) is here modified by assuming as source field the term $\left(-\frac{M(\xi)-M^\tau}{I_E^*}\right)$

$$\chi = \int_0^L \Phi_{L_c}(x-\xi, L_c)\left(-\frac{M(\xi)-M^{\tau}}{I_E^*}\right)d\xi \tag{36}$$

As already discussed, Eq. (36) is equivalent to the following differential equation

$$\left(1-L_c^2\frac{\partial^2}{\partial x^2}\right)\chi = -\frac{M-M^{\tau}}{I_E^*} \tag{37}$$

with the following constitutive boundary conditions (CBCs) at the FG nanobeam ends ($x = 0,L$)

$$-\frac{\partial \chi}{\partial x}(0)+\frac{1}{L_c}\chi(0)=0 \tag{38}$$

$$\frac{\partial \chi}{\partial x}(L)+\frac{1}{L_c}\chi(L)=0 \tag{39}$$

By manipulating Eq. (37), the expression of the stress-driven nonlocal resultant moment incorporating surface effects can be obtained as

$$M = -I_E^*\frac{\partial^2 w}{\partial x^2}+I_E^*L_c^2\frac{\partial^4 w}{\partial x^4}+M^{\tau} \tag{40}$$

Finally, by substituting Eq. (40) into Eq. (26), the governing equation of an inflected FG nanobeam incorporating surface energy effect in terms of transverse displacement is obtained as

$$I_E^*L_c^2\frac{\partial^6 w}{\partial x^6}-I_E^*\frac{\partial^4 w}{\partial x^4}+\mathrm{T}^s\frac{\partial^2 w}{\partial x^2}+q_z=0 \tag{41}$$

with the corresponding constitutive boundary conditions (CBCs) and the standard boundary conditions (SBCs) at the FG nanobeam ends

- SBCs ($x = 0,L$)

$$w = w^*|_{x=0,L} \text{ or } \frac{\partial M}{\partial x}+\mathrm{T}^s\frac{\partial w}{\partial x} = V^*|_{x=0,L} \tag{42}$$

$$-\frac{\partial w}{\partial x} = \frac{\partial w^*}{\partial x}|_{x=0,L} \text{ or } M = M^*|_{x=0,L} \tag{43}$$

- CBCs ($x = 0,L$)

$$-\frac{\partial^3 w}{\partial x^3}\pm\frac{1}{L_c}\frac{\partial^2 w}{\partial x^2}=0 \tag{44}$$

where w^*, V^* and M^* represent assigned displacement, shear force and bending moment at the boundary points ($x = 0,L$), respectively.

Now, by introducing the following dimensionless quantities

$$\widetilde{x} = \frac{x}{L} \tag{45}$$

$$\widetilde{w} = \frac{w}{L} \tag{46}$$

$$\widetilde{w}^* = \frac{w^*}{L} \tag{47}$$

$$\widetilde{V}^* = \frac{V^*L^2}{I_E^*} \tag{48}$$

$$\widetilde{M}^* = \frac{M^*L}{I_E^*} \tag{49}$$

$$\widetilde{q}_z = \frac{q_zL^3}{I_E^*} \tag{50}$$

Table 1
Material parameter of iron film on glass substrate.

Material	Parameters	Values	Unit
Iron film on glass substrate (M1)	E^B	56.25	[GPa]
	E^S	23	[N/m]
	τ^S	110	[N/m]

$$\theta = \frac{\mathrm{T}^S L^2}{I_E^*} \tag{51}$$

$$\widetilde{M}^{\tau} = \frac{M^{\tau} L}{I_E^*} \tag{52}$$

the SSDM dimensionless governing equations of the bending problem for a FG nanobeam can be formulated as follow

- Equilibrium equation

$$\lambda_c^2 \frac{\partial^6 \widetilde{w}}{\partial \widetilde{x}^6} - \frac{\partial^4 \widetilde{w}}{\partial \widetilde{x}^4} + \theta \frac{\partial^2 \widetilde{w}}{\partial \widetilde{x}^2} + \widetilde{q}_z = 0 \tag{53}$$

- SBCs ($\widetilde{x} = 0,\ 1$)

$$\widetilde{w} = \widetilde{w}^*|_{\widetilde{x}=0,1} \text{ or } \frac{\partial \widetilde{M}}{\partial \widetilde{x}} + \theta \frac{\partial \widetilde{w}}{\partial \widetilde{x}} = \widetilde{V}^*|_{\widetilde{x}=0,1} \tag{54}$$

$$-\frac{\partial \widetilde{w}}{\partial \widetilde{x}} = \left.\frac{\partial \widetilde{w}^*}{\partial \widetilde{x}}\right|_{\widetilde{x}=0,1} \text{ or } \widetilde{M} = \widetilde{M}^*|_{\widetilde{x}=0,1} \tag{55}$$

- CBCs ($\widetilde{x} = 0,\ 1$)

$$-\frac{\partial^3 \widetilde{w}}{\partial \widetilde{x}^3} \pm \frac{1}{L_c} \frac{\partial^2 \widetilde{w}}{\partial \widetilde{x}^2} = 0 \tag{56}$$

being $\widetilde{M} = \widetilde{M}(\widetilde{x})$

$$\widetilde{M} = -\frac{\partial^2 \widetilde{w}}{\partial \widetilde{x}^2} + \lambda_c^2 \frac{\partial^4 \widetilde{w}}{\partial \widetilde{x}^4} + \widetilde{M}^{\tau} \tag{57}$$

The general solution of Eq. (53) which describes the deflection of the FG nanobeam including surface effects can be obtained as

$$\widetilde{w}(\widetilde{x}) = -\frac{\widetilde{q}_z \widetilde{x}^2}{2\theta} + \frac{2\mathrm{e}^{\widetilde{x}\, R^-} \lambda_c^2}{1 - \sqrt{1 - 4\theta\lambda_c^2}} C_1 + \frac{2\mathrm{e}^{-\widetilde{x}\, R^-} \lambda_c^2}{1 - \sqrt{1 - 4\theta\lambda_c^2}} C_2 + \frac{2\mathrm{e}^{\widetilde{x}\, R^+} \lambda_c^2}{1 + \sqrt{1 - 4\theta\lambda_c^2}} C_3 + \frac{2\mathrm{e}^{-\widetilde{x}\, R^+} \lambda_c^2}{1 + \sqrt{1 - 4\theta\lambda_c^2}} C_4 + C_5 + \widetilde{x} C_6 \tag{58}$$

where

$$R^- = \frac{\sqrt{\frac{1 - \sqrt{1 - 4\theta\lambda_c^2}}{\lambda_c^2}}}{\sqrt{2}};\ R^+ = \frac{\sqrt{\frac{1 + \sqrt{1 - 4\theta\lambda_c^2}}{\lambda_c^2}}}{\sqrt{2}} \tag{59}$$

The six unknown constants, $C_{i=1\ldots6}$, can be determined by imposing the standard and the constitutive boundary conditions of Eqs. (54)–(56)

5. Results and discussion

This section is divided in two parts: the first one presents a comparison between the results of the proposed approach (SSDM), with and without surface effects, and those published by Mahmoud et al. (2012) in which the Eringen's strain-driven nonlocal model is combined with the surface elasticity theory. In the second part, the effects of surface elastic constants, nonlocal parameter and material gradient index are presented and discussed for two different cross-sectional shapes.

Table 2
Comparison of dimensionless midpoint deflection with previous work for a nonlocal S-S beam.

	M1 – no surface effects [Mahmoud et al.]	[Present]	M1 – surface effects [Mahmoud et al.]	[Present]
0.0+	1.30208	1.30208	1.30204	1.30055
1.0	1.42708	1.20668	1.42703	1.20533
2.0	1.55208	1.13758	1.55203	1.13637
3.0	1.67708	1.08303	1.67703	1.08191
4.0	1.80208	1.03800	1.80202	1.03696

Table 3
Material parameters of metal (m) and ceramic (c).

Material	Parameters	Values	Unit
Ceramic (Si)	E_c^B	210	[GPa]
	E_c^S	-10.6543	[N/m]
	τ_c^S	0.6048	[N/m]
Metal (Al)	E_m^B	70	[GPa]
	E_m^S	5.1882	[N/m]
	τ_m^S	0.9108	[N/m]

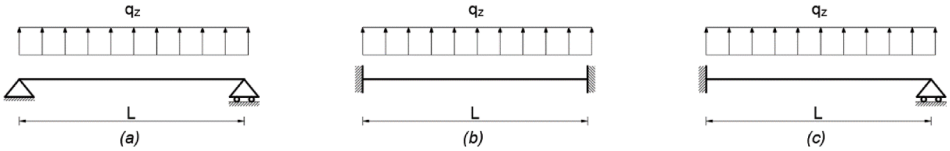

Fig. 2. FG nanobeams under uniformly distributed load with various boundary conditions: (a) Simply-Supported (S-S), (b) Clamped-Clamped (C—C) and (c) Clamped-Pinned (C-P).

5.1. *Model verification*

A nonlocal simply-supported (S-S) beam $(L = 10m, L/h = 100)$ with a square cross-section $(b = h)$ under a uniform distributed load of unit amplitude, as studied in Mahmoud et al. (2012), having the homogenous material M1 (Table 1) given in Gurtin & Murdoch (1975; 1978), has been considered for the model verification.

The comparison is presented in Table 2 in terms of dimensionless midpoint deflection of the nonlocal S-S beam, by setting $L_c^2 \in \{0.0+, 1.0, 2.0, 3.0, 4.0\}$. As can be noted, the obtained results are identycal to those of Mahmoud et al. when both small and surface effects are neglected.

Moreover, it is noticed that as L_c^2 increases, a softening response is exhibited by the model of Mahmoud et al., while a stiffening behavior is obtained with the proposed approach with and without surface effects. As already argued in (Barretta et al., 2018a; Barretta et al., 2018; Romano et al., 2017; Romano & Barretta, 2017), the choice to model nanobeams using the Eringen's strain-driven nonlocal model can lead to physically unacceptable structural solutions. On the contrary, the proposed approach, based on the stress-driven nonlocal model, is a consistent approach to address the size-dependent static behavior of nanobeams. In addition, surface effects determine an abatement of the dimensionless midpoint deflection, for all values of L_c^2, in agreement with the results available in literature (Mahmoud et al., 2012).

5.2. *Effects of surface elastic constants, nonlocal parameter and material gradient index*

In this section, the results of a parametric analysis are presented to show the effectiveness of the proposed approach (SSDM) for the study of the bending behavior of a straight Bernoulli-Euler FG nanobeam, with length $L = 10\ nm$, having two different cross-sectional shapes: a rectangular cross-section, of thickness $h = 0.1L = 1nm$ and width $b = h$, and a circular cross-section, with a value of the diameter D equal to $1.142\ nm$ chosen to ensure the equality of the second moment of area about the principal axis of geometric inertia y of the two considered cross-sectional shapes. The material properties of the FG nanobeam are listed in Table 3.

The analysis has been carried out using both SDM and SSDM formulations and imposing three different boundary conditions at the ends of the FG nanobeam (Fig. 2) subjected to a uniformly distributed load $(q_z = 0.1N/m)$: Simply-Supported (S-S), Clamped-Clamped (C—C) and Clamped-Pinned (C-P)

The dimensionless scale parameters are $\lambda_c \in \{0.00+, 0.10, 0.20, 0.30, 0.40, 0.50\}$ and $k \in \{0, 1, 2, 3\}$. It is worth nothing that, when $k = 0$, the material properties of bulk and surface layer tend to those of a pure ceramic component. On the contrary, as the index $k \to \infty$, the material reduces to a pure metal.

Table 4
Dimensionless midpoint deflection ($\widetilde{w}(1/2)\cdot 10^3$) vs nonlocal parameter λ_c for Simply-Supported (S-S) FG nanobeams with both a rectangular and a circular cross-section under uniformly distributed load for different types of FG material (k).

		$k=0$		$k=1$		$k=2$		$k=3$	
λ_c		Rectangular	Circular	Rectangular	Circular	Rectangular	Circular	Rectangular	Circular
0.00+	SDM	74.5986	74.5986	112.0438	112.0050	124.5473	128.0720	131.9073	137.9670
	SSDM	16.5359	48.7290	19.5345	70.6415	19.6204	78.2813	19.5022	81.8579
0.10	SDM	69.1328	69.1328	103.8340	103.7990	115.4218	118.6880	122.2425	127.8580
	SSDM	15.3069	46.6062	18.5114	69.2848	18.6783	77.3810	18.6027	81.2519
0.20	SDM	59.4689	59.4689	89.3197	89.2892	99.2873	102.0970	105.1546	109.9850
	SSDM	13.3203	42.4098	16.6326	65.9503	16.8495	74.8276	16.7927	79.2808
0.30	SDM	50.8544	50.8544	76.3811	76.3550	84.9048	87.3074	89.9222	94.0528
	SSDM	11.7502	38.2240	15.0992	62.0594	15.3419	71.5837	15.2907	76.5876
0.40	SDM	44.0127	44.0127	66.1051	66.0825	73.4821	75.5614	77.8244	81.3993
	SSDM	10.5684	34.5677	13.9396	58.2800	14.2099	68.2726	14.1691	73.7348
0.50	SDM	38.6396	38.6396	58.0350	58.0151	64.5113	66.3368	68.3236	71.4621
	SSDM	9.64798	31.4621	13.0324	54.7983	13.3326	65.1087	13.3065	70.9397

Table 5
Dimensionless midpoint deflection ($\widetilde{w}(1/2)\cdot 10^3$) vs nonlocal parameter λ_c for Clamped-Clamped (C—C) FG nanobeams with both a rectangular and a circular cross-section under uniformly distributed load for different types of FG material (k).

		$k=0$		$k=1$		$k=2$		$k=3$	
λ_c		Rectangular	Circular	Rectangular	Circular	Rectangular	Circular	Rectangular	Circular
0.00+	SDM	14.9197	14.9197	22.4088	22.4011	24.9095	25.6143	26.3815	27.5933
	SSDM	15.9177	14.1684	20.7212	24.5744	21.8841	31.7697	22.5211	37.0312
0.10	SDM	8.4975	8.4975	12.7629	12.7585	14.1871	14.5886	15.0255	15.7157
	SSDM	10.5781	8.5624	14.8873	15.9821	16.1039	21.6386	16.7914	26.1121
0.20	SDM	4.4599	4.4599	6.6985	6.6962	7.4460	7.6567	7.8861	8.2483
	SSDM	6.3469	4.7086	9.7400	9.3867	10.8577	13.3201	11.5189	16.7076
0.30	SDM	2.5887	2.5887	3.8881	3.8867	4.3220	4.4443	4.5774	4.7876
	SSDM	3.9447	2.7945	6.3818	5.7650	7.2598	8.4025	7.7962	10.7913
0.40	SDM	1.6590	1.6590	2.4918	2.4909	2.7698	2.8482	2.9335	3.0683
	SSDM	2.6194	1.8110	4.3673	3.8035	5.0295	5.6255	5.4421	7.3229
0.50	SDM	1.1452	1.1452	1.7200	1.7194	1.9120	1.9661	2.0250	2.1180
	SSDM	1.8448	1.2578	3.1313	2.6687	3.6335	3.9809	3.9503	5.2238

Table 6
Dimensionless midpoint deflection ($\widetilde{w}(1/2)\cdot 10^3$) vs nonlocal parameter λ_c for Clamped-Pinned (C-P) FG nanobeams with both a rectangular and a circular cross-section under uniformly distributed load for different types of FG material (k).

		$k=0$		$k=1$		$k=2$		$k=3$	
λ_c		Rectangular	Circular	Rectangular	Circular	Rectangular	Circular	Rectangular	Circular
0.00+	SDM	29.8394	29.8394	44.8175	44.8022	49.8189	51.2286	52.7629	55.1866
	SSDM	16.1524	24.9967	20.2281	41.4932	20.9232	50.0164	21.2258	55.3188
0.10	SDM	21.1502	21.1502	31.7667	31.7559	35.3117	36.3110	37.3985	39.1164
	SSDM	12.1966	18.8177	16.2840	33.4630	17.1244	41.5517	17.5196	46.8526
0.20	SDM	13.7432	13.7432	20.6417	20.6347	22.9452	23.5945	24.3012	25.4175
	SSDM	8.4237	13.0720	12.1642	25.3112	13.0546	32.7362	13.4938	37.9513
0.30	SDM	9.2573	9.2573	13.9040	13.8993	15.4556	15.8930	16.3690	17.1209
	SSDM	5.9132	9.2182	9.0954	19.0462	9.9222	25.5117	10.3391	30.3391
0.40	SDM	6.5673	6.5673	9.8638	9.8604	10.9646	11.2748	11.6125	12.1459
	SSDM	4.3093	6.7371	6.9618	14.5704	7.6962	20.0512	8.0726	24.3481
0.50	SDM	4.8726	4.8726	7.3184	7.3159	8.1351	8.3653	8.6159	9.0117
	SSDM	3.2529	5.0982	5.4586	11.3864	6.1003	15.9904	6.4342	19.7386

The dimensionless midpoint deflections of the three different static schemes (S-S, C—C, C-P) of the FG nanobeams are summarized in Tables 4-6 for both rectangular and circular cross-sections, respectively.

The effect of the gradient index, k, on the non-dimensional midpoint deflection, $\widetilde{w}(1/2)$, setting $\lambda_c \in \{0.00+, 0.10, 0.50\}$, for both SSDM (a) and SDM (b) models of elasticity, are plotted in Figs. 3–5, for a rectangular cross-section, and in Figs. 6–8, for a circular cross-section, respectively.

Moreover, the curves of the non-dimensional transverse displacements of the three static schemes of the FG nanobeams (S-S, C—C, C-P) obtained via SDM and SSDM formulations are plotted in the following figures:

- Figs. 9–11, for a rectangular cross-section, setting $\lambda_c \in \{0.00+, 0.10, 0.50\}$ and $k = 2$;

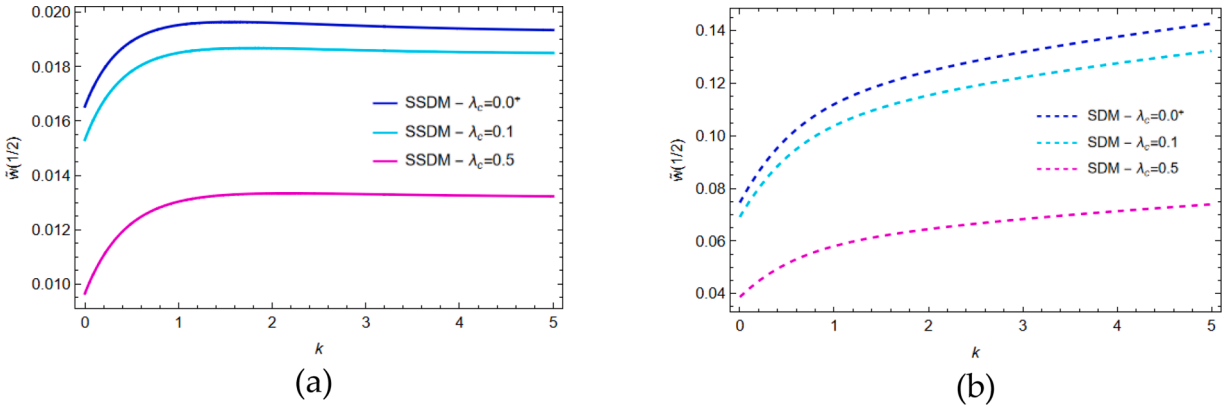

Fig. 3. Effect of the gradient index, k, on non-dimensional midpoint deflection, $\widetilde{w}(1/2)$, of a Simply-Supported (S-S) FG nanobeam with a rectangular cross-section setting $\lambda_c \in \{0.00+, 0.10, 0.50\}$ for both SSDM (a) and SDM (b) models of elasticity.

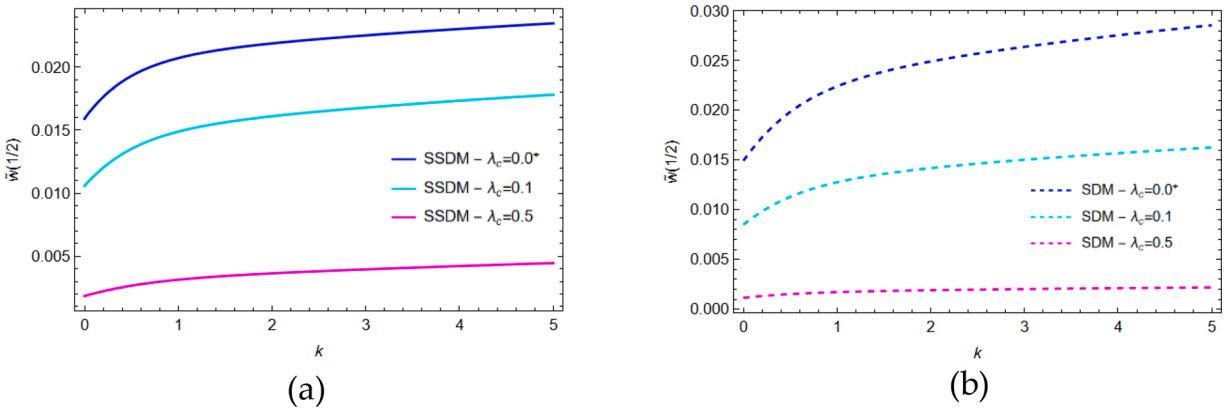

Fig. 4. Effect of the gradient index, k, on non-dimensional midpoint deflection, $\widetilde{w}(1/2)$, of a Clamped-Clamped (C—C) FG nanobeam with a rectangular cross-section setting $\lambda_c \in \{0.00+, 0.10, 0.50\}$ for both SSDM (a) and SDM (b) models of elasticity.

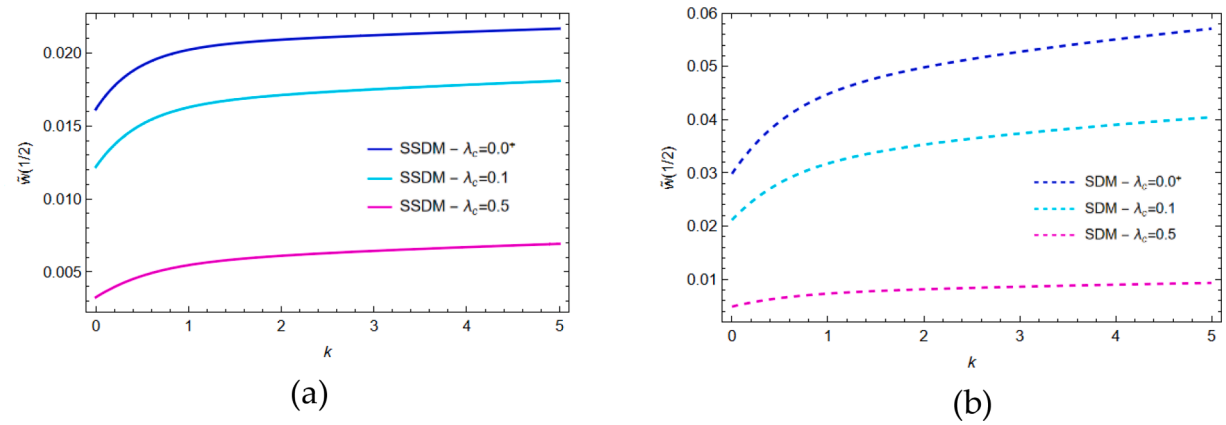

Fig. 5. Effect of the gradient index, k, on non-dimensional midpoint deflection, $\widetilde{w}(1/2)$, of a Clamped-Pinned (C-P) FG nanobeam with a rectangular cross-section setting $\lambda_c \in \{0.00+, 0.10, 0.50\}$ for both SSDM (a) and SDM (b) models of elasticity.

- Figs. 12–14, for a circular cross-section, setting $\lambda_c \in \{0.00+, 0.10, 0.50\}$ and $k = 2$;
- Figs. 15–17, for a rectangular cross-section, setting $k \in \{0, 1, 2, 3\}$ and $\lambda c = 0.3$;
- Figs. 18–20, for a circular cross-section, setting $k \in \{0, 1, 2, 3, \}$ and $\lambda c = 0.3$.

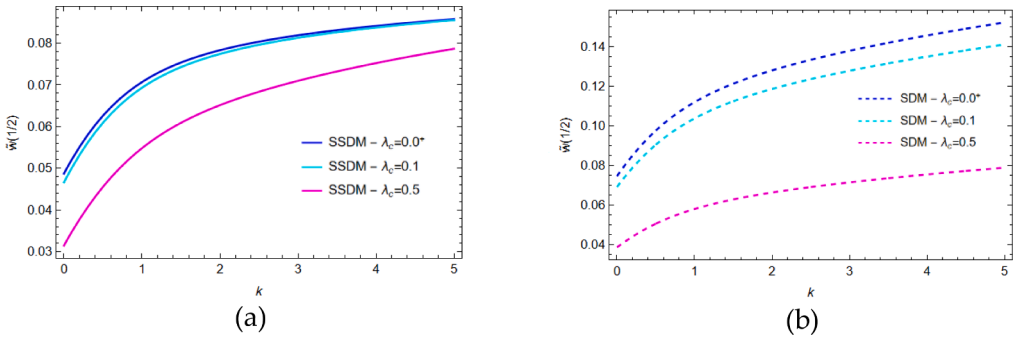

Fig. 6. Effect of the gradient index, k, on non-dimensional midpoint deflection, $\widetilde{w}(1/2)$, of a Simply-Supported (S-S) FG nanobeam with a circular cross-section setting $\lambda_c \in \{0.00+, 0.10, 0.50\}$ for both SSDM (a) and SDM (b) models of elasticity.

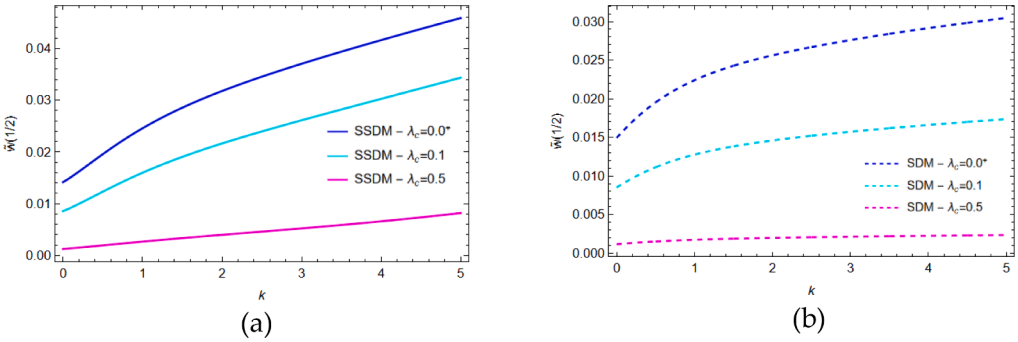

Fig. 7. Effect of the gradient index, k, on non-dimensional midpoint deflection, $\widetilde{w}(1/2)$, of a Clamped-Clamped (C—C) FG nanobeam with a circular cross-section setting $\lambda_c \in \{0.00+, 0.10, 0.50\}$ for both SSDM (a) and SDM (b) models of elasticity.

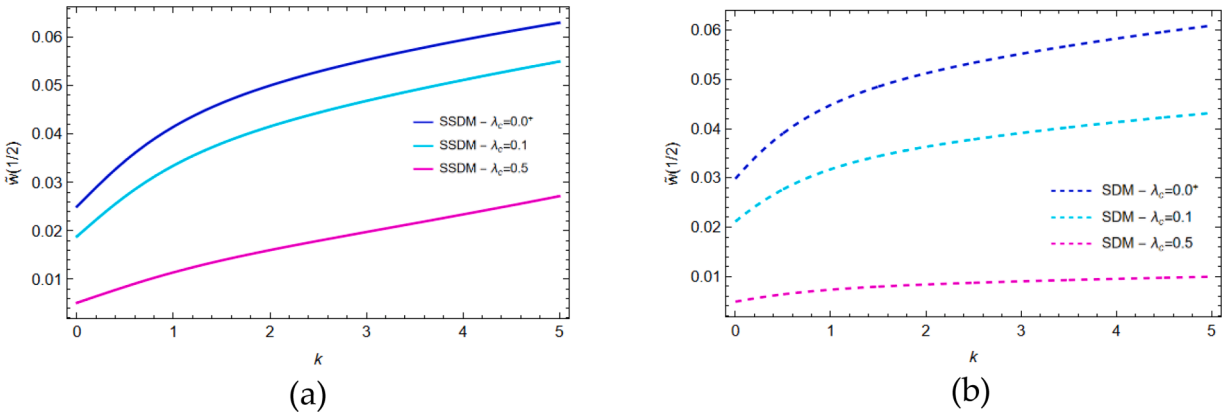

Fig. 8. Effect of the gradient index, k, on non-dimensional midpoint deflection, $\widetilde{w}(1/2)$, of a Clamped-Pinned (C-P) FG nanobeam with a circular cross-section setting $\lambda_c \in \{0.00+, 0.10, 0.50\}$ for both SSDM (a) and SDM (b) models of elasticity.

6. Conclusions

The bending response of Bernoulli-Euler nanobeams subjected to a uniformly distributed load and made of a metal-ceramic functionally graded material has been investigated in this paper by a novel approach based on the stress-driven nonlocal model in conjunction with the surface elasticity theory. In particular, the analysis has been carried out by imposing different boundary conditions at the ends of FG nanobeams with different cross-sectional shapes. Some comparisons with the results available in literature are also presented for the verification of the proposed model.

In view of the numerical results obtained in the present work, the following conclusions may be formulated:

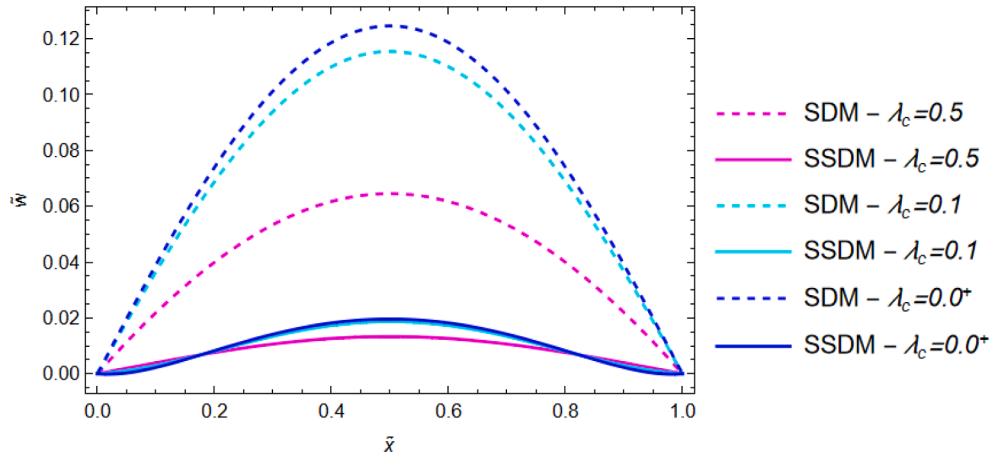

Fig. 9. SSDM and SDM non-dimensional transverse displacements of a Simply-Supported (S-S) FG nanobeam with a rectangular cross-section setting $\lambda_c \in \{0.00+, 0.10, 0.50\}$ and $k = 2$.

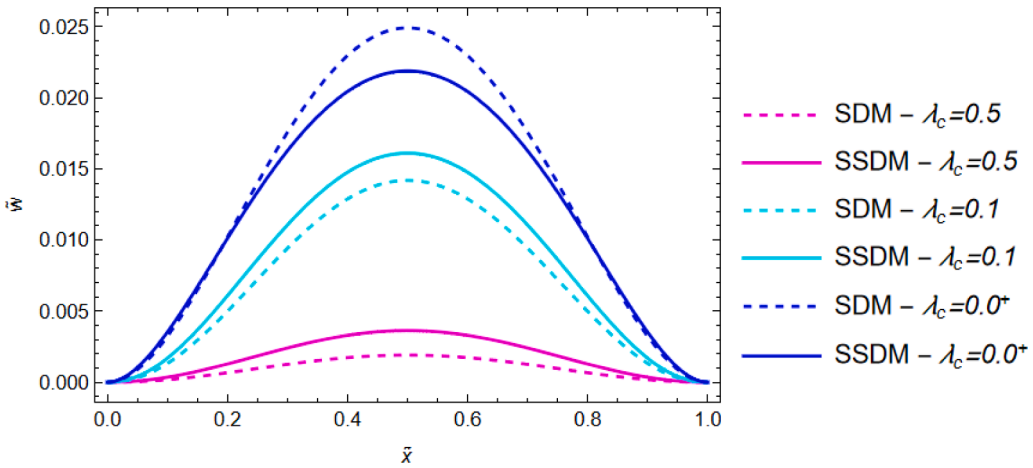

Fig. 10. Comparison between SSDM and SDM non-dimensional transverse displacements of a Clamped-Clamped (C—C) FG nanobeam with a rectangular cross-section setting $\lambda_c \in \{0.00+, 0.10, 0.50\}$ and $k = 2$.

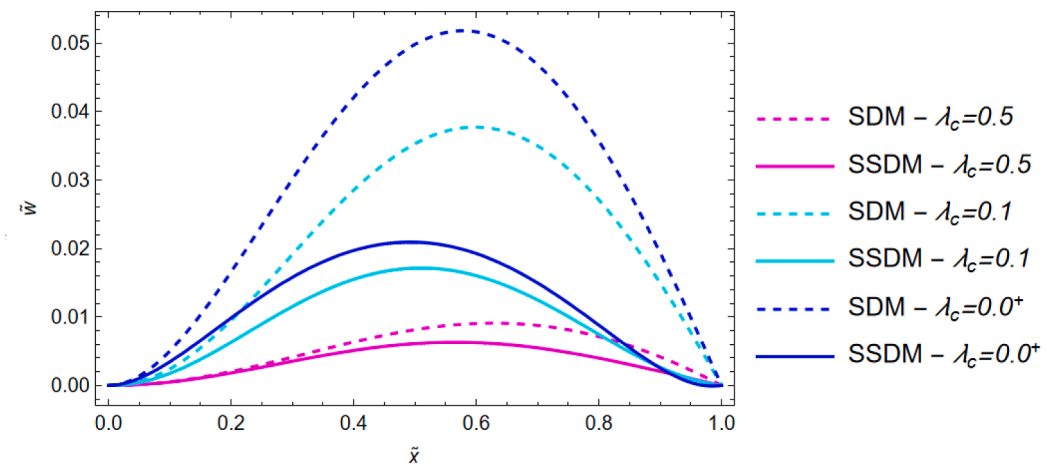

Fig. 11. Comparison between SSDM and SDM non-dimensional transverse displacements of a Clamped-Pinned (C-P) FG nanobeam with a rectangular cross-section setting $\lambda_c \in \{0.00+, 0.10, 0.50\}$ and $k = 2$.

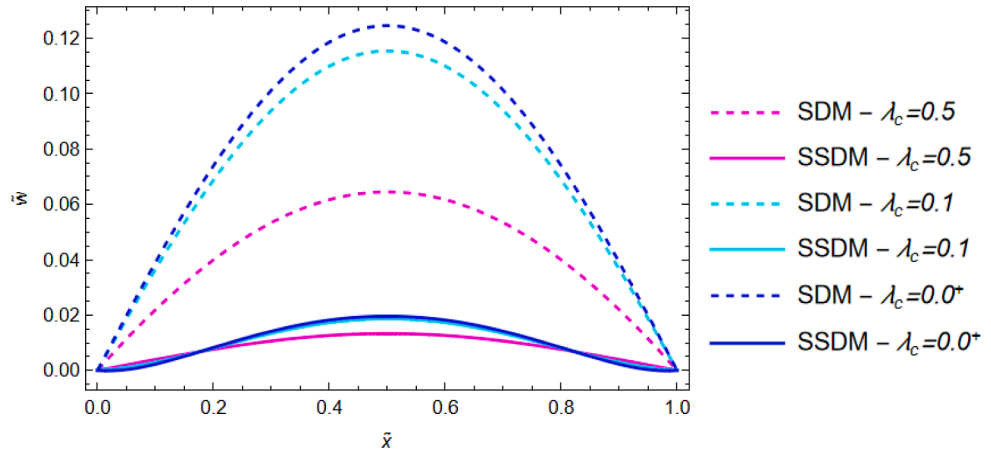

Fig. 12. Comparison between SSDM and SDM non-dimensional transverse displacements of a Simply-Supported (S-S) FG nanobeam with a circular cross-section setting $\lambda_c \in \{0.00+, 0.10, 0.50\}$ and $k = 2$.

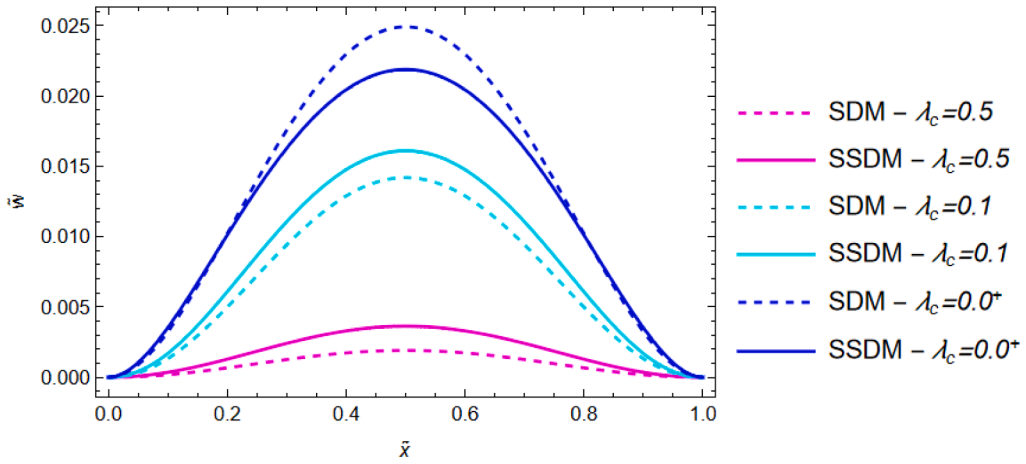

Fig. 13. Comparison between SSDM and SDM non-dimensional transverse displacements of a Clamped-Clamped (C—C) FG nanobeam with a circular cross-section setting $\lambda_c \in \{0.00+, 0.10, 0.50\}$ and $k = 2$.

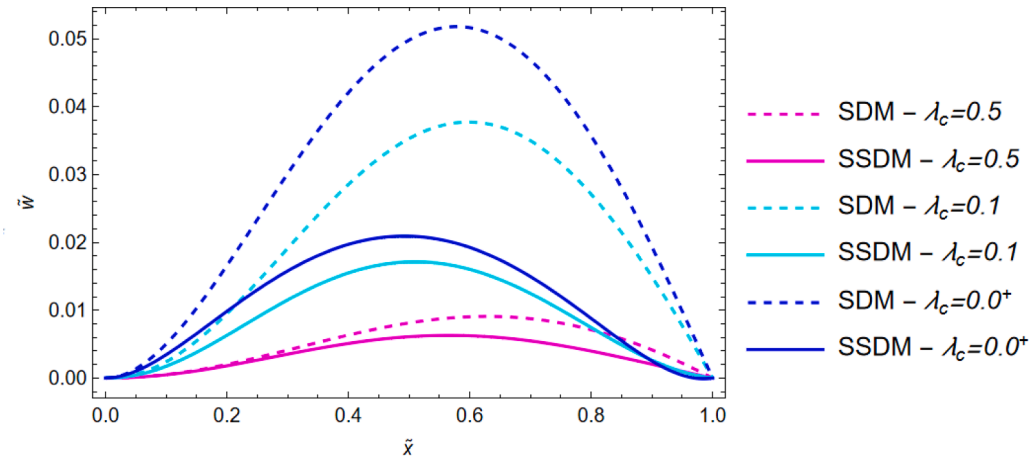

Fig. 14. Comparison between SSDM and SDM non-dimensional transverse displacements of a Clamped-Pinned (C-P) FG nanobeam with a circular cross-section setting $\lambda_c \in \{0.00+, 0.10, 0.50\}$ and $k = 2$.

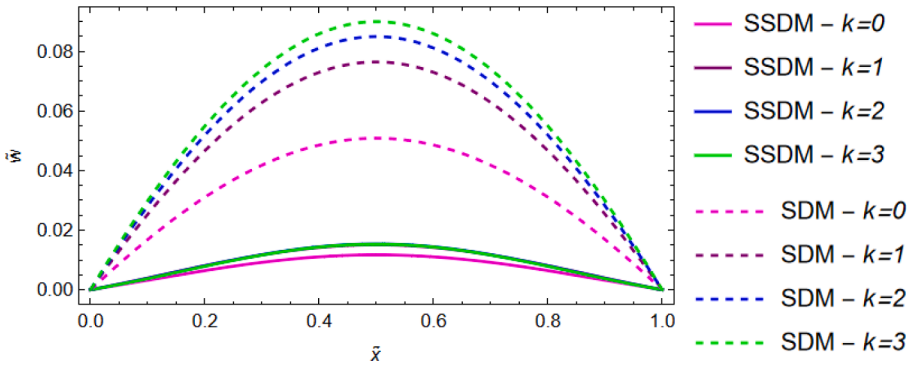

Fig. 15. Comparison between SSDM and SDM non-dimensional transverse displacements of a Simply-Supported (S-S) FG nanobeam with a rectangular cross-section setting $k \in \{0,\ 1,\ 2, 3\}$ and $\lambda_c = 0.3$.

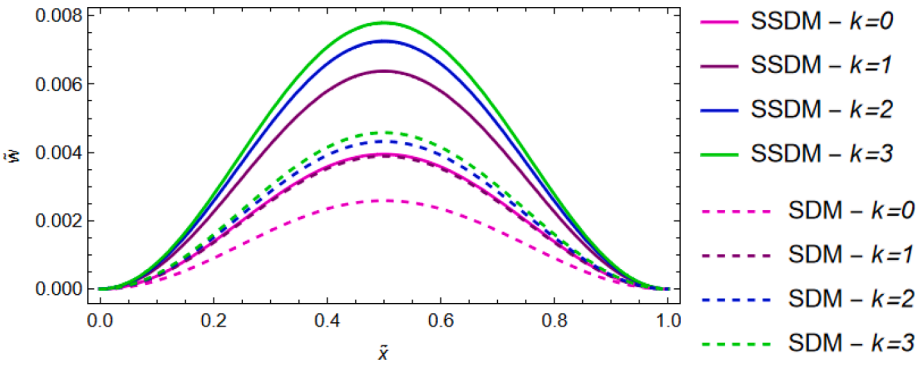

Fig. 16. Comparison between SSDM and SDM non-dimensional transverse displacements of a Clamped-Clamped (C—C) FG nanobeam with a rectangular cross-section setting $k \in \{0,\ 1,\ 2, 3\}$ and $\lambda_c = 0.3$.

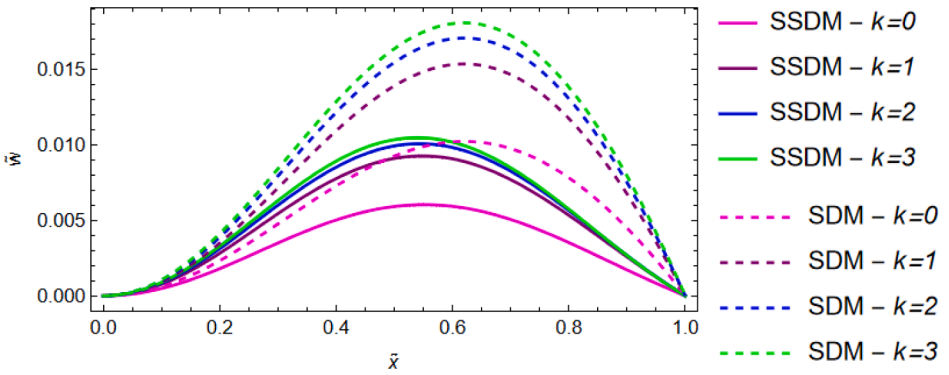

Fig. 17. Comparison between SSDM and SDM non-dimensional transverse displacements of a Clamped-Pinned (C-P) FG nanobeam with a rectangular cross-section setting $k \in \{0,\ 1,\ 2, 3\}$ and $\lambda_c = 0.3$.

- as expected, when the effects of surface energy are neglected, the results obtained with the proposed approach (SSDM) always coincide with those provided by the SDM model;
- as the nonlocal parameter increases, a stiffening nonlocal behavior has been observed, with and without surface effects, both for rectangular and circular cross-sections, no matter what ends conditions are considered;
- when the material gradient index increases, the bending response obtained by employing the SDM formulation is always characterized by a softening trend; the modified static boundary conditions introduced in the proposed model (SSDM) to incorporate surface energy effects determine a more general bending behavior depending on the coupled effects of the nonlocal parameter and the material gradient index, as well as on the cross-sectional shapes.

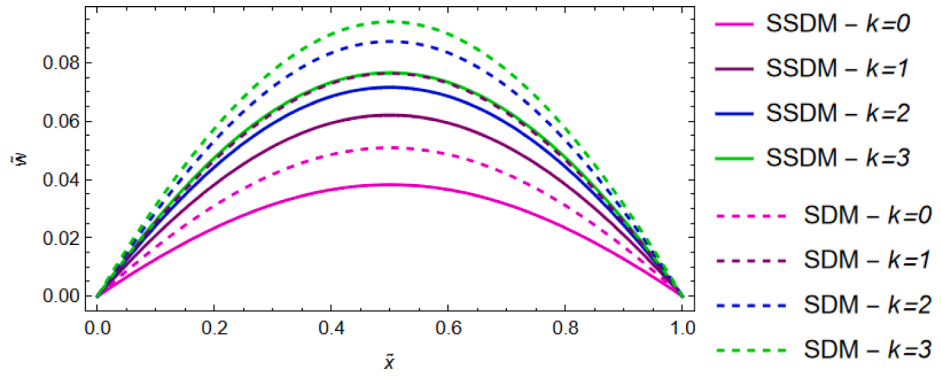

Fig. 18. Comparison between SSDM and SDM non-dimensional transverse displacements of a Simply-Supported (S-S) FG nanobeam with a circular cross-section setting $k \in \{0,\ 1,\ 2, 3\}$ and $\lambda_c = 0.3$.

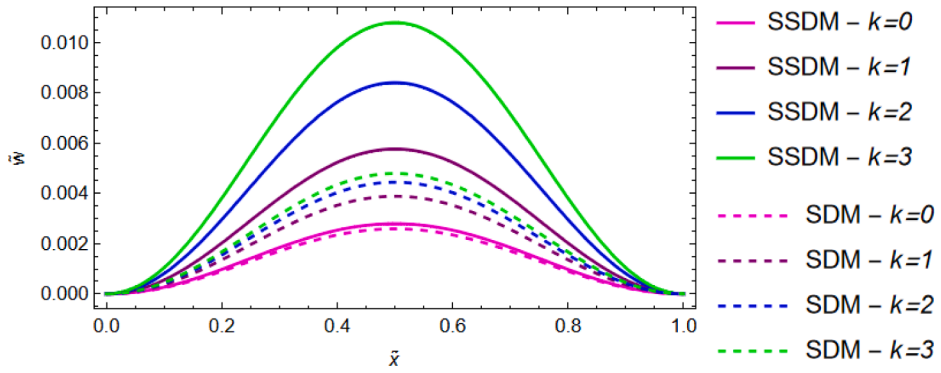

Fig. 19. Comparison between SSDM and SDM non-dimensional transverse displacements of a Clamped-Clamped (C—C) FG nanobeam with a circular cross-section setting $k \in \{0,\ 1,\ 2, 3\}$ and $\lambda_c = 0.3$.

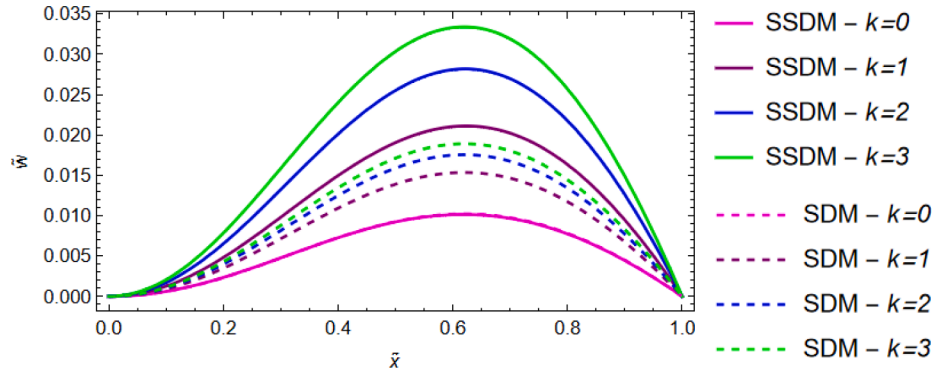

Fig. 20. Comparison between SSDM and SDM non-dimensional transverse displacements of a Clamped-Pinned (C-P) FG nanobeam with a circular cross-section setting $k \in \{0,\ 1,\ 2, 3\}$ and $\lambda_c = 0.3$.

In conclusion, the results have highlighted that the proposed model is suitable for studying surface energy effects on the overall bending behavior of functionally graded Bernoulli-Euler nanobeams with different cross-sectional shaped and represents a reference point for engineering and researchers involved in the design of nano-scaled structures such as nano electromechanical systems and biosensors.

Declaration of Competing Interest

The author declares that she has no known competing financial interests or personal relationships that could have appeared to influence the work reported in this paper.

Data availability

Data will be made available on request.

Acknowledgements

The author gratefully acknowledges the financial support of the Italian Ministry of University and Research (MUR), Research Grant PRIN 2020 No. 2020EBLPLS on “Opportunities and challenges of nanotechnology in advanced and green construction materials”.

References

Akhavan, H., Ghadiri, M., & Zajkani, A. (2019a). A new model for the cantilever MEMS actuator in magnetorheological elastomer cored sandwich form considering the fringing field and casimir effects. *Mechanical Systems and Signal Processing, 121*, 551–561.
Akhavan, H., Ghadiri, M., & Zajkani, A. (2019b). A new model for the cantilever MEMS actuator in magnetorheological elastomer cored sandwich form considering the fringing field and casimir effects. *Mechanical Systems and Signal Processing, 12*, 551–561.
Apuzzo, A., Barretta, R., Luciano, R., Marotti de Sciarra, F., & Penna, R. (2017). Free vibrations of Bernoulli-Euler nano-beams by the stress-driven nonlocal integral model. *Composites Part B (Engineering), 123*, 105–111.
Barretta, R., Faghidian, S. A., Luciano, R., Medaglia, C. M., & Penna, R. (2018). Stress-driven two phase integral elasticity for torsion of nano-beams. *Compos B, 145*, 62–69.
Barretta, R., Čanadija, M., Feo, L., Luciano, R., Marotti de Sciarra, F., & Penna, R. (1 June 2018). Exact solutions of inflected functionally graded nano-beams in integral elasticity. *Composites Part B: Engineering. Volume, 142*, 273–286.
Barretta, R., Čanađija, M., Luciano, R., & Marotti de Sciarra, F. (2022). On the mechanics of nanobeams on nano-foundations. *International Journal of Engineering Science, 180*, Article 103747.
Barretta, R., & Marotti de Sciarra, F. (2019). Variational nonlocal gradient elasticity for nanobeams. *International Journal of Engineering Science, 143*, 73–91.
Barretta, R., Marotti de Sciarra, F., & Vaccaro, M. S. (2019). On nonlocal mechanics of curved elastic beams. *International Journal of Engineering Science, 144*, Article 103140.
Billinge, S. J. L., & Levin, I. (2007). The problem with determining atomic structure at the nanoscale. *Science (New York, N.Y.), 316*, 561–565.
Caporale, A., Darban, H., & Luciano, R. (1 March 2022). Nonlocal strain and stress gradient elasticity of Timoshenko nano-beams with loading discontinuities. *International Journal of Engineering Science. Volume, 173*, Article 103620.
Chandel, V. S., Wang, G., & Talha, M. (2020). Advances in modelling and analysis of nano structures: A review. *Nanotechnology Reviews, 9*, 230–258.
Chen, Q., Pugno, N., & Li, Z. (2013). Influence of surface stress on elastic constants of nanohoneycombs. *Physica E, 53*, 217–222.
Cornacchia, F., Fabbrocino, F., Fantuzzi, N., Luciano, R., & Penna, R. (2021). Analytical solution of cross- and angle-ply nano plates with strain gradient theory for linear vibrations and buckling. *Mechanics of Advanced Materials and Structures, 28*(12), 1201-121.
Darban, H., Fabbrocino, F., Feo, L., & Luciano, R. (2020). Size-dependent buckling analysis of nanobeams resting on two-parameter elastic foundation through stress-driven nonlocal elasticity model. Mechanics of Advanced Materials and Structures. *Mech Adv Mater Struct*, 1–9.
Dastjerdi, S., Alibakhshi, A., Akgöz, B., & Civalek, Ö. (1 February 2023). On a comprehensive analysis for mechanical problems of spherical structures. *International Journal of Engineering Science. Volume, 183*, Article 103796.
Dastjerdi, S., Malikan, M., Akgöz, B., Civalek, Ö., Wiczenbach, T., & Eremeyev, V. A. (2022). On the deformation and frequency analyses of SARS-CoV-2 at nanoscale. *International Journal of Engineering Science, 170*, Article 103604.
Eringen, A. (1972). Linear theory of nonlocal elasticity and dispersion of plane waves. *International journal of engineering science, 10*(5), 425–435.
Eringen, A. (1983). On differential equations of nonlocal elasticity and solutions of screw dislocation and surface waves. *Journal of applied physics, 54*, 4703–4710.
Eringen, A. C. (1987). Theory of nonlocal elasticity and some applications. *Research Mechanics, 21*, 313–342.
Eyvazian, A., Shahsavari, D., & Karami, B. (September 2020). On the dynamic of graphene reinforced nanocomposite cylindrical shells subjected to a moving harmonic load. *International Journal of Engineering Science. Volume, 154*, Article 103339.
Farajpour, A., Ghayesh, M. H., & Farokhi, H. (1 August 2022). A review on the mechanics of nanostructures. *International Journal of Engineering Science. V., 178*, Article 103724.
Fernández-Sáez, J., Zaera, R., Loya, J. A., & Reddy, J. N. (2016). Bending of Euler–Bernoulli beams using Eringen’s integral formulation: A paradox resolved. *International Journal of Engineering Science, 99*, 107–116.
Ghadiri, M., Shafiei, N., & Akbarshahi, A. (2016). Influence of thermal and surface effects on vibration behavior of nonlocal rotating Timoshenko nanobeam. *Appl. Phys. A, 122*, 673. 10.1007/s00339-016-0196-3.
Ghayesh, M. H., & Farajpour, A. (2019). A review on the mechanics of functionally graded nanoscale and microscale structures. *International Journal of Engineering Science, 137*, 8–36.
Gurtin, M., & Murdoch, A. (1975). A continuum theory of elastic material surfaces. *Archive for Rational Mechanics and Analysis, 57*(4), 291–323.
Gurtin, M., & Murdoch, A. (1978). Surface stress in solids. *International Journal of Solids and Structures, 14*(6), 431–440.
Hashemian, M., Foroutan, S., & Toghraie, D. (2019). Comprehensive beam models for buckling and bending behavior of simple nanobeam based on nonlocal strain gradient theory and surface effects. *Mechanics of Materials, 139*, Article 103209.
He, J., & Lilley, C. M. (2008). Surface effect on the elastic behavior of static bending nanowires. *Nano Letters, 8*(7), 1798–1802.
Hui, D. W., & Gang-Feng, W. (2011). Surface Effects on the Vibration and Buckling of Double-Nanobeam-Systems. *Hindawi Publishing Corporation Journal of Nanomaterials Volume*. https://doi.org/10.1155/2011/518706. Article ID 518706, 7 pages.
Kekic T., Barisic I. Computational and Structural Biotechnology Journal (2020), 18, 1191–1201.
Lam, D. C. C., Yang, F., Chong, A. C. M., Wang, J., & Tong, P. (2003). Experiments and theory in strain gradient elasticity. *Journal of the Mechanics and Physics of Solids, 51*, 477–508.
Li, C., Yao, L., Chen, W., & Li, S. (2015). Comments on nonlocal effects in nano-cantilever beams. *International Journal of Engineering Science, 87*, 47–57.
Li, L., & Hu, Y. (2022). A nonlocal surface theory for surface–bulk interactions and its application to mechanics of nanobeams. *International Journal of Engineering Science, 172*, Article 103624.
Li, L., Lin, R., & Ng, T. Y. (2020). Contribution of nonlocality to surface elasticity. *International Journal of Engineering Science, 152*, Article 103311.
Lim, C., Zhang, G., & Reddy, J. N. (2015). A higher-order nonlocal elasticity and strain gradient theory and its applications in wave propagation. *Journal of the Mechanics and Physics of Solids, 78*, 298–313.
Mahmoud, F. F., Eltaher, M. A., Alshorbagy, A. E., & Meletis, E. I (2012). Static analysis of nanobeams including surface effects by nonlocal finite element. *Journal of Mechanical Science and Technology, 26*(11), 3555–3563.
Malikan, M., & Eremeyev, V. A. (1 May 2022). On a flexomagnetic behavior of composite structures. *International Journal of Engineering Science. Volume, 175*, Article 103671.
Malikan, M., Uglov, N. S., & Eremeyev, V. A. (2020). On instabilities and post-buckling of piezomagnetic and flexomagnetic nanostructures. *International Journal of Engineering Science, 157*, Article 103395.

Maranganti, R., & Sharma, P. (2007). A novel atomistic approach to determine strain gradient elasticity constants: Tabulation and comparison for various metals, semiconductors, silica, polymers and their relevance for nanotechnologies. *J Mech Phys Sol, 55*, 1823–1852.
Mindlin, R. (1968). Micro-structure in linear elasticity. *Archive for Rational Mechanics and Analysis, 16*(1), 51–78.
Penna, R., Feo, L., & Lovisi, G. (2021a). Hygro-thermal bending behavior of porous FG nano-beams via local/nonlocal strain and stress gradient theories of elasticity. *Composite Structures, 263*, Article 113627.
Penna, R., Feo, L., Fortunato, A., & Luciano, R. (2021b). Nonlinear free vibrations analysis of geometrically imperfect FG nano-beams based on stress-driven nonlocal elasticity with initial pretension force. *Composite Structures, 255*, Article 112856.
Penna, R., Feo, L., Lovisi, G., & Fabbrocino, F. (2021c). Hygro-thermal vibrations of porous FG nano-beams based on local/nonlocal stress gradient theory of elasticity. *Nanomaterials, 11*, 910. https://doi.org/10.3390/nano11040910
Penna, R., Lovisi, G., & Feo, L. (2021d). Dynamic response of multilayered polymer functionally graded carbon nanotube reinforced composite (FG-CNTRC) nano-beams in hygro-thermal environment. *Polymers, 13*, 2340. https://doi.org/10.3390/polym13142340
Rafii-Tabar, H., Ghavanloo, E., & Fazelzadeh, S. A. (2016). Nonlocal continuum-based modeling of mechanical characteristics of nanoscopic structures. *Physics Reports, 638*, 1–97.
Ren, Y.-. M., & Qing, H. (2021). Bending and buckling analysis of functionally graded Euler–Bernoulli beam using stress-driven nonlocal integral model with bi-Helmholtz kernel. *International Journal of Applied Mechanics, 13*, Article 2150041.
Rezaiee-Pajand, M., & Rajabzadeh-Safaei, N. (1 August 2022). Stress-driven nonlinear behavior of curved nanobeams. *International Journal of Engineering Science, 178*, Article 103724. V.
Romano, G., & Barretta, R. (2016). Comment on the paper ‘‘Exact solution of Eringen’s nonlocal integral model for bending of Euler–Bernoulli and Timoshenko beams by Meral Tuna & Mesut Kirca’. *International Journal of Engineering Science, 109*, 240–242.
Romano, G., & Barretta, R. (2017). Nonlocal elasticity in nanobeams: The stress-driven integral model. *International Journal of Engineering Science, 115*, 14–27.
Romano, G., Barretta, R., Diaco, M., & Marotti de Sciarra, F. (2017). Constitutive boundary conditions and paradoxes in nonlocal elastic nano-beams. *International Journal of Mechanical Sciences, 121*, 151–156.
Russillo, A. F., & Failla, G. (2022). Wave propagation in stress-driven nonlocal Rayleigh beam lattices. *International Journal of Mechanical Sciences, 215*, Article 106901.
Russillo, A. F., Failla, G., Barretta, R., & Marotti de Sciarra, F. (2022). On the dynamics of 3D nonlocal solids. *International Journal of Engineering Science, 180*, Article 103742. Volume.
Saffari, S., Hashemian, M., & Toghraie, D. (2017). Dynamic stability of functionally graded nanobeam based on nonlocal Timoshenko theory considering surface effects. *Physica B, 520*, 97–105.
Shahmohammadi, M. A., Mirfatah, S. M., Salehipour, H., & Civalek, Ö. (1 January 2023). On nonlinear forced vibration of micro scaled panels. *International Journal of Engineering Science Volume, 182*, Article 103774.
Shenoy V.B. Physical Review B: Condensed Matter 71 (2005) 094104.
Sourani, P., Hashemian, M., Pirmoradian, M., & Toghraie, D. (2020). A comparison of the Bolotin and incremental harmonic balance methods in the dynamic stability analysis of an Euler–Bernoulli nanobeam based on the nonlocal strain gradient theory and surface effects. *Mechanics of Materials, 145*, Article 103403.
Vaccaro, M. S. (2022). On geometrically nonlinear mechanics of nanocomposite beams. *International Journal of Engineering Science, 173*, Article 103653.
Wang, G. F., & Feng, X. Q. (2009). Timoshenko beam model for buckling and vibration of nanowires with surface effects. *Journal of Physics D, Applied Physics,, 42*, Article 155411.
Wang, J., Duan, H., Huang, Z., & Karihaloo, B. L. (2006). A scaling law for properties of nano-structured materials. *Proceedings of the Royal Society A: Mathematical, Physical and Engineering Sciences, 462*(2069), 1355–1363.
Xu, X., Karami, B., & Shahsavari, D. (1 March 2021). International Journal of Engineering Science. *Time-dependent behavior of porous curved nanobeam, 160*, Article 103455.
Yang, W., Wang, S., Kang, W., Yu, T., & Li, Y. (2023). A unified high-order model for size-dependent vibration of nanobeam based on nonlocal strain/stress gradient elasticity with surface effect. *International Journal of Engineering Science, 182*, Article 103785.
Yee, K., Mergen, H., & Ghayesh, M. H. (1 May 2023). A review on the mechanics of graphene nanoplatelets reinforced structures. *International Journal of Engineering Science, 186*, Article 103831. Volume.
Zheng, Y., Karami, B., & Shahsavari, D. (1 August 2022). On the vibration dynamics of heterogeneous panels under arbitrary boundary conditions. *International Journal of Engineering Science. Volume, 178*, Article 103727.
Zhu, X., & Li, L. (2019). A well-posed Euler-Bernoulli beam model incorporating nonlocality and surface energy effect. *Appl. Math. Mech. -Engl. Ed., 40*(11), 1561–1588.